Lung (2025) 203:39
https://doi.org/10.1007/s00408-025-00791-w

RESEARCH

ACUTE LUNG INJURY

FLRT3 Overexpression Attenuates Ischemia–Reperfusion Induced Vascular Hyperpermeability and Lung Injury Through RND3

Yongmei Cao[1] · Shiyang Sheng[1] · Yong Zhong[2] · Jiawei Shang[3] · Cui Jin[3] · Qin Tan[3] · Feng Ping[3] · Weifeng Huang[3] · Yongchao Liu[1] · Yingchuan Li[1]

Received: 9 October 2024 / Accepted: 10 February 2025

Abstract

Purpose Pulmonary ischemia/reperfusion injury (IRI) causes endothelial barrier dysfunction and increased vascular permeability. Fibronectin leucine-rich transmembrane protein-3 (FLRT3) is known to regulate endothelial cell function, but its role in pulmonary IRI remains unexplored.

Methods We established both a mouse lung I/R model and a hypoxia/reoxygenation (H/R) cell culture model using human pulmonary microvascular endothelial cells (HPMECs). The effects of FLRT3 manipulation were assessed through lentiviral-mediated overexpression and knockdown approaches. Lung injury was evaluated by histological analysis, immunohistochemistry, and lung injury scoring. Endothelial barrier function was assessed using transmission electron microscopy, Evans blue extravasation, and endothelial permeability assays.

Results FLRT3 expression was predominantly localized in pulmonary endothelial cells and was downregulated following I/R injury. Lentiviral vectors overexpressing FLRT3 (LV-FLRT3, 1×10^9 TU/ml) via tail vein injection before I/R surgery. FLRT3 overexpression effectively protected against lung injury by maintaining vascular integrity and reducing edema formation in I/R-challenged mice. In H/R-treated HPMECs, we identified that FLRT3 protein underwent autophagic-lysosomal degradation. Mechanistically, FLRT3 preserved endothelial barrier function through interaction with Rho family GTPase 3 (RND3), which prevented RhoA pathway-mediated cytoskeletal disruption. FLRT3 overexpression in HPMECs promoted cell migration, maintained cytoskeletal structure, and reduced endothelial hyperpermeability under H/R conditions. Importantly, RND3 knockdown in vivo significantly attenuated FLRT3's protective effects against I/R injury, as evidenced by increased lung injury scores, vascular permeability, and RhoA pathway activation.

Conclusions Our findings reveal FLRT3, a critical regulator of endothelial barrier function during IRI through the RND3-RhoA pathway, is a potential therapeutic target for pulmonary IRI.

Keywords Lung ischemia/reperfusion · FLRT3 · RND3 · Cytoskeletal rearrangement · Vascular permeability

Yongmei Cao, Shiyang Sheng and Yong Zhong contributed equally to the work.

✉ Weifeng Huang
breeze-huang@hotmail.com

✉ Yongchao Liu
liuyongchao@tongji.edu.cn

✉ Yingchuan Li
yingchuan_li@tongji.edu.cn

[1] Department of Critical Care Medicine, Shanghai Tenth People'S Hospital, Tongji University School of Medicine, No. 301, Middle Yanchang Road, Jingan District, Shanghai 200072, China

[2] Clinical Nuclear Medicine Center, Imaging Clinical Medical Center, Institute of Nuclear Medicine, Department of Nuclear Medicine, Shanghai Tenth People'S Hospital, Tongji University School of Medicine, Shanghai 200072, China

[3] Department of Critical Care Medicine, Shanghai Sixth People'S Hospital Affiliated to Shanghai Jiao Tong University School of Medicine, No. 605, Yishan Road, Xuhui District, Shanghai 200233, China

Published online: 06 March 2025

Introduction

Pulmonary ischemia/reperfusion (I/R) injury (IRI) occurs in response to cardiopulmonary bypass cardiac surgery [1], lung transplantation [2, 3], high-volume resuscitation [4], pulmonary embolism [5] and single lung ventilation [6]. IRI is characterized by inflammation, alveolar damage, hypoxemia and vascular permeability, which often lead to pulmonary edema and reduced oxygenation. In lung transplantation patients, IRI can lead to primary graft dysfunction, which is a major cause of mortality and morbidity post-surgery [7]. IRI also results in prolonged hospital stays, which contributes to higher mortality and morbidity, as well as an increased financial burden on the patient and healthcare system [8]. Current options for managing IRI patients are unsatisfactory and thus, the development of novel therapeutic strategies to treat IRI is required.

In response to lung IRI, activation of the immune system and subsequent release of reactive oxygen species leads to pulmonary vascular endothelial cell dysfunction and disruption of the endothelial barrier [9, 10]. Endothelial barrier dysfunction promotes migration of inflammatory cells to the injured tissue, further potentiating I/R damage [11–13]. Loss of barrier function also leads to increased vascular permeability. Indeed, pulmonary edema, a significant pathological complication, is directly linked to heightened vascular permeability [14, 15]. Since vascular permeability is a critical risk factor in lung I/R-induced complications, it may be a potential target to exploit in the development of novel therapeutic strategies [16].

The cytoskeletal structure is critical in the regulation of endothelial barrier integrity and vascular permeability [17–20] with disruptions to both the actin filaments and microtubule networks leading to the breakdown of tight junction protein complexes and subsequent paracellular gap formation, which contribute to increased permeability [21, 22]. Inflammation can lead to the rapid reorganization of actin filaments, which can cause junction destabilization and subsequent inflammatory cell migration into tissues [21, 23]. Key regulators of the actin filaments and, therefore, vascular permeability are the Rho subfamily of small GTPases [24–26]. Thus, inflammatory cell modulation of the RhoA kinase pathway is a critical aspect of endothelial barrier integrity.

In response to endothelial barrier injury, the vascular repair process mediates restoration of a functional endothelial monolayer and re-establishment of endothelial cell–cell junctions to reform a semi-permeable barrier [27]. These endothelial regeneration processes involve the migration and proliferation of resident endothelial cells [28]. Although a role for Rho GTPases has been described in regulating endothelial migration [29–31] and restoration of the endothelial barrier [32], the molecular pathways that control endothelial cell actin dynamics, endothelial cell migration, endothelial cell–cell junctions and vascular permeability remain poorly defined. A better understanding of the pathways that regulate endothelial cell structure and permeability may provide new ways to prevent tissue damage and edema following I/R.

Fibronectin leucine-rich transmembrane protein-3 (FLRT3) is expressed on endothelial cells and is important for endothelial cell survival, migration and tube formation [33]. Interestingly, FLRT3 has been shown to be downregulated in human thoracic visceral adipose tissue before and after lung reperfusion [34], suggesting a potential role in lung I/R. However, the expression patterns and role of FLRT3 in lung tissue during lung I/R have yet to be elucidated.

Here, we show that FLRT3 is downregulated following lung I/R. Overexpression of FLRT3 protects against I/R-induced damage through interactions with Rho family GTPase 3 (RND3) and inhibition of the RhoA kinase pathway. Our results identify FLRT3 and RND3 as novel therapeutic targets in lung I/R.

Methods

Reagents

Cycloheximide (CHX, S7418) and MG132 (S2619) were purchased from Selleck (Houston, TX, USA). 3-methyladenine (3-MA, M9281), ammonium chloride (NH_4Cl, A9434), chloroquine (CQ, C6628) and the RhoA pathway agonist, U-46619 (D8174) were purchased from Sigma-Aldrich (Munich, Germany).

Construction of Lentiviral Vectors

For in vivo studies, mouse FLRT3 (GenBank accession number NM_001172160) full-length coding sequences were synthesized and subcloned into a GV492 vector (GeneChem). For in vitro studies with HPMECs, human FLRT3 (GenBank accession number NM_013281) full-length coding sequences were used. The results of mouse GV492-FLRT3 and human GV492-FLRT3 vectors were sequenced to confirm correct insertion.

For knockdown experiments, shRNAs targeting FLRT3 or RND3 and a scrambled negative control shRNA were synthesized and cloned into the GV493 vector (GeneChem). The shRNA sequences are given in Table 1. The vectors were co-transfected into 293 T cells using Lipo3000 (Thermo Fisher Scientific, Waltham, MA, USA) according

Table 1 The shRNA sequences used in this study

	Forward (5′–3′)	Reverse (5′–3′)
FLRT3 shRNA	CCGGGCTTGGATGATAATCGCATATCTCGAGATATG CGATTATCATCCAAGCTTTTTG	AATTCAAAAAGCTTGGATGATAATCGCATATCTCGA GATATGCGATTATCATCCAAGC
RND3 shRNA	CCGGCGGACAGATGTTAGTACATTACTCGAGTAATG TACTAACATCTGTCCGTTTTTG	AATTCAAAAACGGACAGATGTTAGTACATTACTCGA GTAATGTACTAACATCTGTCCG
Control shRNA	CCGGCCTAAGGTTAAGTCGCCCTCGCTCGAGCGAGG GCGACTTAACCTTAGGTTTTTG	AATTCAAAAACCTAAGGTTAAGTCGCCCTCGCTCGA GCGAGGGCGACTTAACCTTAGG

to the manufacturer's instructions. After 72 h, the lentiviruses were harvested and stored at − 80 °C.

Animal Model and Experimental Design

Sixty-five male C57BL/6J mice (6–8 weeks old, weighing 20–26 g) from Shanghai SLAC Laboratory Animal Co., Ltd. were housed under standard conditions (22 ± 2 °C, 12 h light/dark cycles). All animal procedures were approved by Shanghai Tenth People's Hospital, Tongji University School of Medicine. To establish the lung I/R model, anesthetized mice (sodium pentobarbital, 50 mg/kg, i.p.) underwent tracheotomy followed by mechanical ventilation (tidal volume 0.6 ml, 120 breaths/min, 1:2 inspiration-to-expiration ratio, 100% oxygen). Left lung ischemia was induced by clamping the left pulmonary hilum for 60 min, followed by reperfusion. Three experimental series were conducted: (1) a time-course study ($n = 20$) with varying reperfusion durations (0, 60, 120, and 240 min, $n = 5$ per group); (2) FLRT3 overexpression study ($n = 20$) comparing Sham, I/R (60 min ischemia, 120 min reperfusion), I/R+LV-control, and I/R+LV-FLRT3 groups ($n = 5$ per group); and (3) RND3 mechanism study ($n = 25$) including Sham, I/R+LV-control, I/R+LV-FLRT3, I/R+LV-FLRT3+sh-control, and I/R+LV-FLRT3+sh-RND3 groups ($n = 5$ per group). For lentiviral interventions, mice received tail vein injections of respective vectors (1×10^9 TU/ml, 100 µl) 3 days before I/R surgery, with successful delivery confirmed by western blot analysis of target protein expression. Sham controls underwent identical procedures without ischemia, while I/R groups experienced 60 min ischemia followed by 120 min reperfusion. The successful delivery was confirmed by examining FLRT3 or RND3 protein expression in lung tissue using western blot. Sham controls underwent identical procedures without ischemia, while I/R groups experienced 60 min ischemia followed by 120 min reperfusion.

Lung Wet-to-Dry Ratio

Pulmonary edema was measured using the lung wet-to-dry ratio method. Briefly, the lower lobe of the left lung was removed and the weight was recorded (wet weight). Samples were dried in a 60 °C incubator for 96 h. Then, the dry weight was measured, and the ratio was calculated.

Immunohistochemistry

Lung tissue sections (5 µm) were deparaffinized, incubated with 3% H_2O_2 in methanol for 15 min, then boiled in citrate buffer (pH 6.0). Samples were blocked with 5% BSA for 30 min at room temperature and incubated overnight with anti-cleaved caspase-3 antibody (1:400; #9661, Cell Signaling Technology, Danvers, MA, USA). After washing in PBS, samples were incubated with horseradish peroxidase (HRP)-conjugated goat anti-rabbit IgG at 37 °C for 30 min, then stained using the DAB detection system kit (ZSGB-Bio, Beijing, China). Cleaved caspase-3 staining was visualized under light microscopy (Olympus, Tokyo, Japan).

Haematoxylin & Eosin (H&E)

Lungs were inflated and fixed (10% neutral-buffered formalin at room temperature for 12–24 h), dehydrated with ethanol and embedded in paraffin. Sections (5 µm) were cut and stained with H&E. The lung injury score was determined based on the following three criteria: (i) aggregation or infiltration of inflammatory cells in vessel walls or air spaces [1 = only wall, 2 = rare cells in air space, 3 = intermediate, and 4 = severe (air space congested)], (ii) hyaline membrane formation and interstitial congestion in the lung [1 = normal lung, 2 = moderate (> 25% of lung section), 3 = intermediate (25%–50% of lung section), and 4 = severe (> 50% of lung section)], and (iii) hemorrhage [0 = absent, and 1 = present] [35]. The sum of the individual scores for each criterion was calculated to obtain the lung injury score for each animal. Sections were independently assessed by two pathologists blinded to the animal grouping.

Evans Blue Dye Assay

For the Evans blue dye assay, 4 ml/kg of 2% Evans blue dye (E2129, Merck KGaA, Darmstadt, Germany) in normal saline was administered through the tail vein 10 h before the animals were humanely killed. After adequate perfusion with normal saline, the Evans blue dye was extracted from the lung using

formamide for 18 h at 60 °C. The absorbance of the supernatant was measured at 620 nm on a microplate reader (BioTek Instruments, Winooski, VT, USA) and was reported as the amount of Evans blue dye per wet tissue weight (μg/g).

Transmission Electron Microscopy (TEM)

Lung tissue samples (1–2 mm cubes) were fixed in 0.1 M sodium cacodylate buffer (pH 7.4) containing 2.5% glutaraldehyde and 2% paraformaldehyde for 2 h at room temperature. Samples were then washed in 0.1 M cacodylate buffer, fixed with 1% OsO_4/1.5% $KFeCN_6$ for 1 h, washed in water, and incubated in 1% aqueous uranyl acetate for 1 h. Next, samples were washed in water, dehydrated in increasing concentrations of alcohol, and incubated in propylene oxide for 1 h. Following overnight incubation in a 1:1 mixture of propylene oxide and TAAB Epon, samples were embedded in TAAB Epon and polymerized at 60 °C for 48 h. Sections (60 nm thin) were cut, placed on copper grids, stained with lead citrate and examined under transmission electron microscope (Tecnai-G220-TWIN TEM, FEI, Holland).

Cell Culture

Human pulmonary microvascular endothelial cells (HPMECs), purchased from ATCC (Manassas, VA, USA), were cultured in endothelial cell medium (ECM, Gibco, USA) containing 10% heat-inactivated fetal bovine serum (FBS, Gibco), 1% endothelial cell growth factor (Beyotime Biotechnology, Jiangsu, China), and 100 IU/ml penicillin and streptomycin (Sigma-Aldrich) at 37 °C in a humidified atmosphere of 5% CO_2.

To mimic lung I/R in vitro, HPMECs were subjected to hypoxia and reoxygenation (H/R). Briefly, when the cell confluency reached approximately 80%, HPMECs were subjected to 12 h hypoxia (1% O_2, 5% CO_2 and 94% N_2) followed by 4 h reoxygenation (5% CO_2, 95% room air) at 37 °C.

Cell Transduction

HPMECs at 70–80% confluence were infected with lentiviral vectors at MOI of 10 in the presence of 5 μg/ml polybrene. After 12 h, the medium was replaced with fresh complete medium. The infection efficiency was confirmed 72 h post-transduction by western blot analysis of target protein expression.

Evans Blue-Albumin Monolayer Permeability Assay In Vitro

HPMECs (1×10^4 cells/well) were seeded into Transwell inserts (pore size 3.0 μm, #3472, Costar, MA, USA) and subjected to various treatments. Permeability was assessed by removing the culture medium from the upper chamber, and replacing it with Evans blue-conjugated albumin (final concentration: 0.67 mg/ml). 4% BSA was added to the lower chamber. The levels of Evans blue-conjugated albumin in the upper chamber and 4% BSA in the lower chamber were kept at the same height to eliminate the impact of hydrostatic pressure gradient. After incubation for 1 h at 37 °C in 5% CO_2, the mixture in the lower chamber was collected, and its absorbance was measured using a microplate reader at a wavelength of 620 nm. The leakage of Evans blue-conjugated albumin from HPMECs was calculated using a standard curve.

Trans-endothelial Electric Resistance (TEER) Measurements

Endothelial barrier integrity was determined using an electrical resistance system (Millicell-ERS, MERS00002; Merck Millipore, Germany). The electric resistance of monolayer HMPECs was measured every 4 h, and the TEER was calculated as described by the manufacturer. A high TEER was representative of a high barrier integrity.

Cell Viability

Cell viability was assessed using Cell Counting Kit-8 (CCK-8; Dojindo, Tokyo, Japan). Cells were seeded into 96-well plates (1×10^4 cells/ml), and subjected to H/R and lentiviral treatments. Samples were incubated with CCK-8 solution for 2 h at 37 °C, and the absorbance was read using a microplate reader at 450 nm.

Wound Healing Assay

HMPECs were seeded into 6-well plates at a density of 1.0×10^5 cells/well. Following treatment of the cells, a 1 ml pipette tip was used to scrap through the cellular monolayer. Cells were then washed gently with PBS to remove cell debris. The medium was replaced and cells were incubated for 24 h at 37 °C in 5% CO_2. Images were captured by microscopy at the 0 and 24 h time points at the same position for each wound. The migration ability was determined by measuring the width of the scratch wound at the different time points.

Transwell Migration Assay

HPMECs (2×10^4 cells/well) were seeded into Transwell plates (pore size: 8.0 μm, #3464, CoStar, Cambridge, MA, USA) in serum-free ECM (100 μl). Following H/R and lentiviral treatments, non-migrating cells on the surface of the insert were removed with a cotton swab, while cells that had

migrated through the Transwell inserts were washed with PBS and fixed in 4% paraformaldehyde for 20 min. Samples were washed three times with PBS, then stained with crystal violet for 10 min and was washed three times with PBS. Samples were visualized by microscopy. The number of cells was counted in three random fields.

Western Blot Analysis

Lung tissue samples and cell samples were lysed in RIPA buffer (Beyotime Biotechnology Shanghai, China) supplemented with protease inhibitors (Roche Applied Science, Indianapolis, IN, USA) for 30 min on ice. Protein concentrations were measured using a BCA Protein Assay Kit (Beyotime Biotechnology). Protein samples were then separated by SDS-PAGE and transferred to PVDF membranes. Membranes were blocked in 5% skim milk in TBST for 1 h at room temperature, then incubated with primary antibodies against FLRT3 (1:1,000; ab223047, Abcam, Cambridge, MA, USA), RND3 (1:500; sc-53874, Santa Cruz Biotechnology, CA, USA), VE-cadherin (1:1,000; ab205336, Abcam), ZO-1 (1:1,000; ab276131, Abcam), claudin-5 (1:5,000; ab131259, Abcam), occludin (1:1,000; ab216327, Abcam), p-MYPT1 (1:500; ab59203, Abcam), MYPT1 (1:1,000; ab59235, Abcam), RhoA (1:5,000; ab187027, Abcam), p-MCL1 (1:1,000; #4579, Cell Signaling Technology), MCL1 (1:1,000; #94296, Cell Signaling Technology) and LC3I/II (1:1,000; #4108, Cell Signaling Technology) overnight at 4 °C. Membranes were washed three times with TBST, and incubated for 1 h at room temperature with HRP-conjugated secondary antibodies. Protein bands were visualized using an Enhanced Chemiluminescence Kit.

RhoA-GTP (Rhotekin-RBD Pull-Down) Assay

GTP-bound RhoA was measured using a RhoA Activation Assay Kit (Merck Millipore, Billerica, USA). Briefly, equal amounts (1,000 µg) of each cell lysate were incubated with 30 µg GST-Rhotekin Rho-binding domain coupled to glutathione-agarose beads for 45 min. The beads were washed three times with washing buffer. Samples were separated by SDS-PAGE and transferred to nitrocellulose membranes. RhoA was detected by western blot using an anti-RhoA antibody (1:1,000; ab187027, Abcam).

GST Pulldown Assay

His-FLRT3 (ProteinTech, Wuhan, China) and GST-RND3 (ProteinTech) fusion proteins were mixed in GST-binding buffer for 12 h at 4 °C. Then, anti-His or anti-GST beads were added to the fusion proteins and incubated for 4 h. The beads were washed three times and eluted proteins were subjected to western blot analysis.

Co-immunoprecipitation (Co-IP)

Protein was extracted using lysis buffer, and incubated with primary antibodies against FLRT3 (1:100; #3462, Cell Signaling Technology), RND3 (1:100; sc-53874, Santa Cruz Biotechnology) and IgG at 4 °C overnight. The following day, samples were incubated with protein Dynabeads (50 µl; Thermo Fisher Scientific) for 6 h at 4 °C. After washing three times with RIPA buffer, IP lysates (20 µl) were added to 2× loading buffer, boiled, and subjected to western blot analysis.

F-actin Staining

Changes in cytoskeletal structure were monitored by immunofluorescence staining of F-actin. Briefly, HPMECs were fixed with 4% paraformaldehyde, permeabilized with 0.3% Triton X-100, then stained with fluorescein isothiocyanate (FITC)-conjugated phalloidin (Molecular Probes, Eugene, OR, USA). After washing with PBST four times, cells were visualized using FluorSave reagent (Calbiochem, Billenica, MA, USA) with a fluorescent microscope (Olympus).

Real-Time Quantitative Reverse Transcription PCR (qRT-PCR)

RNA was extracted from lung tissue and HPMECs using the RNeasy Mini Kit according to the manufacturer's instructions (Qiagen, Valencia, CA, USA). cDNA was generated and qRT-PCR was performed using the Quantitect SYBR Green RT-PCR kit with the ABI 7300 real time PCR system (Applied Biosystems, Foster City, CA, USA). The following primers were used: human FLRT3: 5′-CGACAGCAGGACAAGCTCA-3′/5′-TCAGAACCCAGGAAGACGAGA-3′; mouse FLRT3: 5′-AGTCAACTGGATGCTCTCGC-3′/5′-GTAAAAACCCTCCCCCGTCT-3′.

Immunofluorescence Microscopy

Lung lobes were removed from mice and placed in 4% paraformaldehyde in PBS at 4 °C overnight. Fixed lungs were paraffin embedded, and 5-µm sections were obtained. Serial lung sections were subjected to dewaxing followed by antigen retrieval (Antigen Unmasking Solution, Vector Laboratories, Burlingame, CA, USA) and blocking for 1 h in 5% normal goat serum, 0.2% Triton X-100, and 0.05% fish skin gelatin. Lung sections were stained with anti-FLRT3 (1:100; ab223047 Abcam) and anti-CD31 (1:100; ab76533, Abcam) antibodies at 4 °C overnight.

HPMECs were washed in PBS, fixed in 10% neutral-buffered formalin for 15 min at 37 °C, then permeabilized with Target Retrieval Solution (Dako, Carpinteria, CA, USA) for 10 min at 95 °C. After cooling, samples were blocked

with 1% BSA in PBS containing 0.05% Tween-20 (PBST) at 37 °C for 1 h, then incubated with anti-FLRT3 (1:100; ab223047, Abcam), anti-VE-cadherin (1:1,000; ab205336, Abcam) and anti-claudin-5 (1:500; ab131259, Abcam) antibodies for one hour at 37 °C. Next, samples were incubated with fluorescein isothiocyanate (FITC)-conjugated secondary antibodies (1:50, Jackson ImmunoResearch, West Grove, PA, USA) at 4 °C overnight. Finally, samples were mounted using Vectashield Mounting Medium with DAPI (Vector Laboratories) and examined by fluorescence microscopy (Olympus). Images were captured and analyzed using cellSens image analysis software (Olympus).

Statistical Analysis

Data are presented as mean ± SD. An unpaired Student's *t* test was used to analyze statistically significant differences among two groups. One-way ANOVA and Tukey's multiple comparisons test were used to analyze statistically significant differences among multiple groups. Two-way ANOVA with Tukey's post hoc test was used to analyze multiple groups with two categorical variables. Statistical analyses were performed using GraphPad Prism Software version 8.0 (San Diego, CA, USA). *P*-values < 0.05 were considered to be statistically significant.

Results

Overexpression of FLRT3 Ameliorates Lung Vascular Permeability Induced by Lung I/R

To determine the role of FLRT3 in lung IRI, we first examined FLRT3 expression levels in the lung tissue of mice after I/R. FLRT3 protein expression was significant downregulated at 60 and 120 min after reperfusion in the lung tissue compared to Sham-control (Fig. 1A). Since the most significant decrease in FLRT3 occurred 120 min post-reperfusion, subsequent experiments were based on this time point. We next used immunofluorescence staining to determine the expression pattern of FLRT3. We found that FLRT3 was predominantly expressed in pulmonary endothelial CD31-positive cells, and that FLRT3 expression levels were significantly reduced in I/R mice (Fig. 1B).

Since FLRT3 expression was decreased following I/R, we next examined whether overexpressing FLRT3 could protect against the damage caused by lung I/R, mice were treated with LV-FLRT3 via tail vein injection 3 days before I/R surgery. First, we confirmed that FLRT3 expression was significantly increased in I/R mice following treatment with lentiviral vectors overexpressing FLRT3 (LV-FLRT3) (Fig. 1C), with FLRT3 expression levels in I/R+LV-FLRT3 mice similar to those observed in Sham mice. H&E staining (Fig. 1D), as well as immunohistochemical staining of cleaved-caspase 3 (Fig. 1E), revealed that compared to Sham mice, I/R mice displayed aggravated lung tissue injury and increased apoptosis, while LV-FLRT3 treatment mitigated cell injury and inhibited apoptosis. We further demonstrated that LV-FLRT3 treatment protected the lung from I/R injury by increasing the PaO_2/FiO_2 ratio (Fig. 1F) and reducing the lung wet-to-dry weight ratio (Fig. 1G) compared to I/R+LV-Control. Evans blue dye assay indicated that LV-FLRT3 treatment also significantly reduced vascular permeability compared to I/R+LV-Control (Fig. 1H). Finally, the junctional integrity of the pulmonary endothelium was analyzed by TEM. The junctions between pulmonary endothelial cells were found to be tight and characterized by closely apposed membranes in the lungs of Sham mice, while cell–cell junctions were found to be disrupted with increased space between adjacent cell membranes in the lungs of I/R mice. LV-FLRT3 treatment of I/R mice resulted in increased cell–cell junctional integrity (Fig. 1I). Together, these results demonstrate that during lung IRI, reduced expression of FLRT3 on endothelial cells results in vascular permeability, lung edema and organ dysfunction.

Overexpression of FLRT3 Promotes Cell Migration and Rescues H/R-Induced Cell Death and Inhibition on Cell Migration

Repair of the endothelial barrier following I/R requires endothelial regeneration that promote migration and proliferation of resident endothelial cells[28]. To examine the mechanisms through which FLRT3 regulates vascular permeability, we next examined the effects of FLRT3 overexpression or knockdown on wound healing and cell migration in H/R-treated HPMECs, which acted as an in vitro model of I/R. As shown in Fig. 2A, significantly higher FLRT3 protein expression levels were observed in HPMECs transduced with LV-FLRT3, while LV-shFLRT3 significantly reduced FLRT3 protein expression. Cell viability was not affected by the overexpression or knockdown of FLRT3 (Fig. 2B). However, wound healing (Fig. 2C) and cell migration (Fig. 2D) were significantly increased in FLRT3-overexpressing cells, and significantly decreased in FLRT3-silenced cells.

Since our data indicated that FLRT3 overexpression promoted wound healing and cell migration in HPMECs, we next asked whether overexpressing FLRT3 could protect against H/R-induced cellular injury. As expected, H/R led to a reduction in FLRT3 expression levels in HPMECs, while overexpression of FLRT3 restored FLRT3 protein expression levels in H/R-treated cells to control cell levels (Fig. 2E). H/R led to reduced cell viability and cell migration (Fig. 2F–H), which were partially rescued following FLRT3 overexpression (Fig. 2F). Wound healing and Transwell assays revealed that H/R led to a reduction in cell

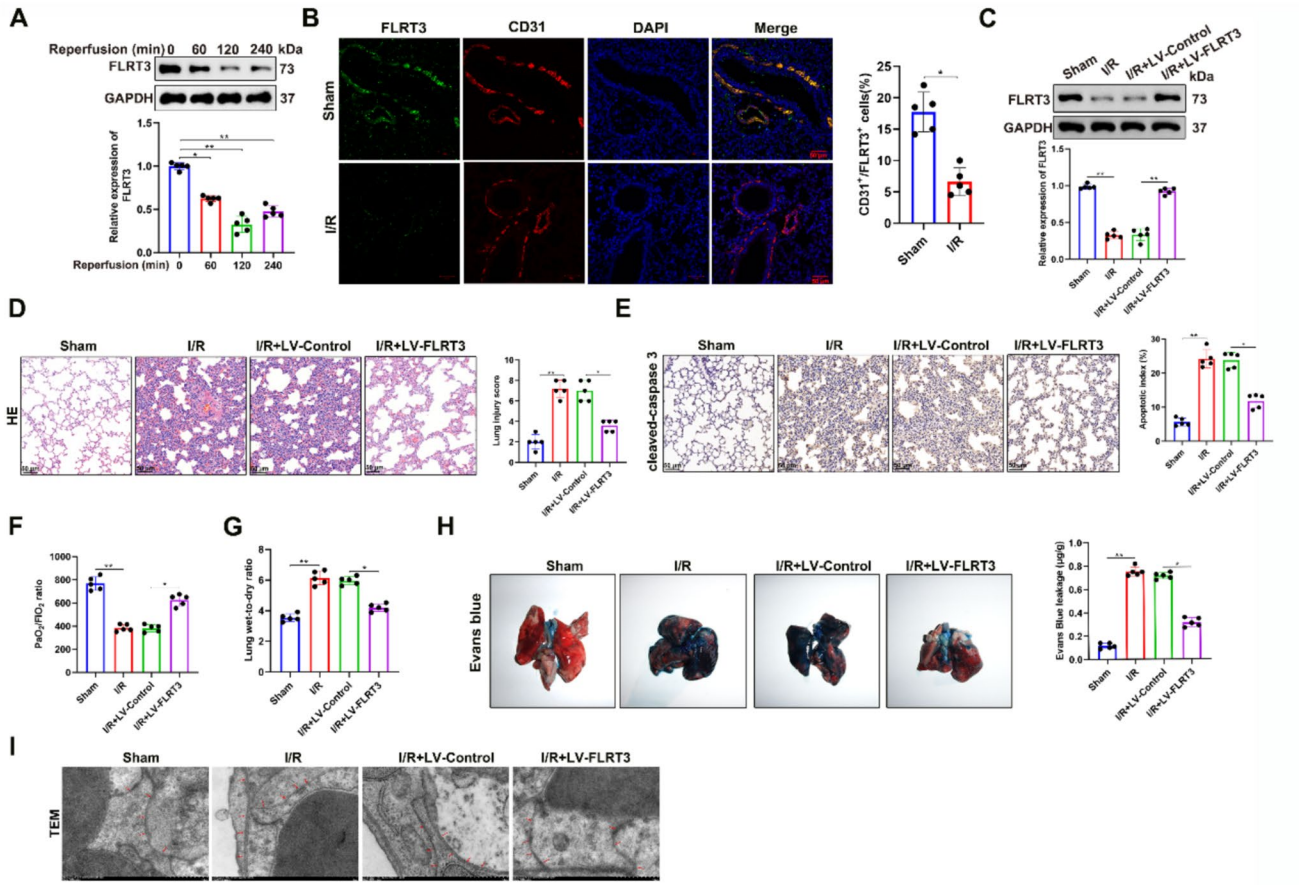

Fig. 1 of FLRT3 ameliorates lung vascular permeability induced by lung I/R. Mouse left lungs were subjected to 60 min ischemia via helium clamp followed by different durations of reperfusion (R60 min, R120 min, and R240 min). **A** Western blot analysis revealed decreased FLRT3 protein levels at 60 and 120 min post-reperfusion. **B** Double immunofluorescence staining showed FLRT3 (green) co-localized with CD31 (red) in pulmonary vessels and decreased after I/R. Scale bar, 50 μm. **C** Western blot confirmed successful FLRT3 restoration in mice receiving LV-FLRT3 compared to LV-Control. **D** H&E staining showed FLRT3 overexpression attenuated I/R-induced tissue damage and inflammatory infiltration. **E** Immunohistochemical staining of cleaved caspase 3 demonstrated reduced apoptosis with FLRT3 overexpression. Scale bar, 50 μm. **F** Blood gas analysis revealed improved PaO_2/FiO_2 ratio with FLRT3 overexpression. **G** Wet-to-dry ratio measurement showed decreased pulmonary edema with FLRT3 overexpression). **H** Evans blue extravasation assay demonstrated preserved vascular barrier function with FLRT3 overexpression. **I** TEM imaging revealed maintained endothelial cell–cell junctions in FLRT3-overexpressing mice. Data are presented as mean ± SD. $n = 5$ per group. Statistical significance was determined using unpaired Student's t test to compare two groups, and one-way ANOVA and Tukey's multiple comparisons tests to compare multiple groups. $^{*}P < 0.05$, $^{**}P < 0.01$ compared with the indicated groups.

migration, which was rescued following overexpression of FLRT3 (Fig. 2G, H). Taken together, our findings suggest that FLRT3 has a role in mediating endothelial cell migration during H/R in HPMECs.

FLRT3 Overexpression Increases Endothelial Barrier Integrity via Cytoskeletal Remodeling and Restoration of Cell–Cell Junctions After H/R

The migration of endothelial cells, which is a key process in the restoration of endothelial barrier integrity and regulation of vascular permeability, requires changes in actin cytoskeleton and cell–cell junctions [29–31]. Thus, we next examined the effects of H/R and FLRT3 overexpression on the integrity of the endothelial barrier and endothelial cell cytoskeletal structure in vitro in HPMECs. As expected, H/R led to a decrease in TEER, which was representative of a loss in barrier integrity. However, overexpression of FLRT3 significantly increased TEER in H/R-treated cells, suggesting that FLRT3 is involved in maintaining endothelial barrier integrity (Fig. 3A). At the same time, Evans blue dye assay revealed that leakage of the endothelial barrier was increased following H/R, while overexpression of FLRT3 significantly reduced H/R-induced barrier leakage (Fig. 3B). Together, these findings suggest that overexpression of FLRT3 prevents H/R-induced loss of endothelial barrier integrity.

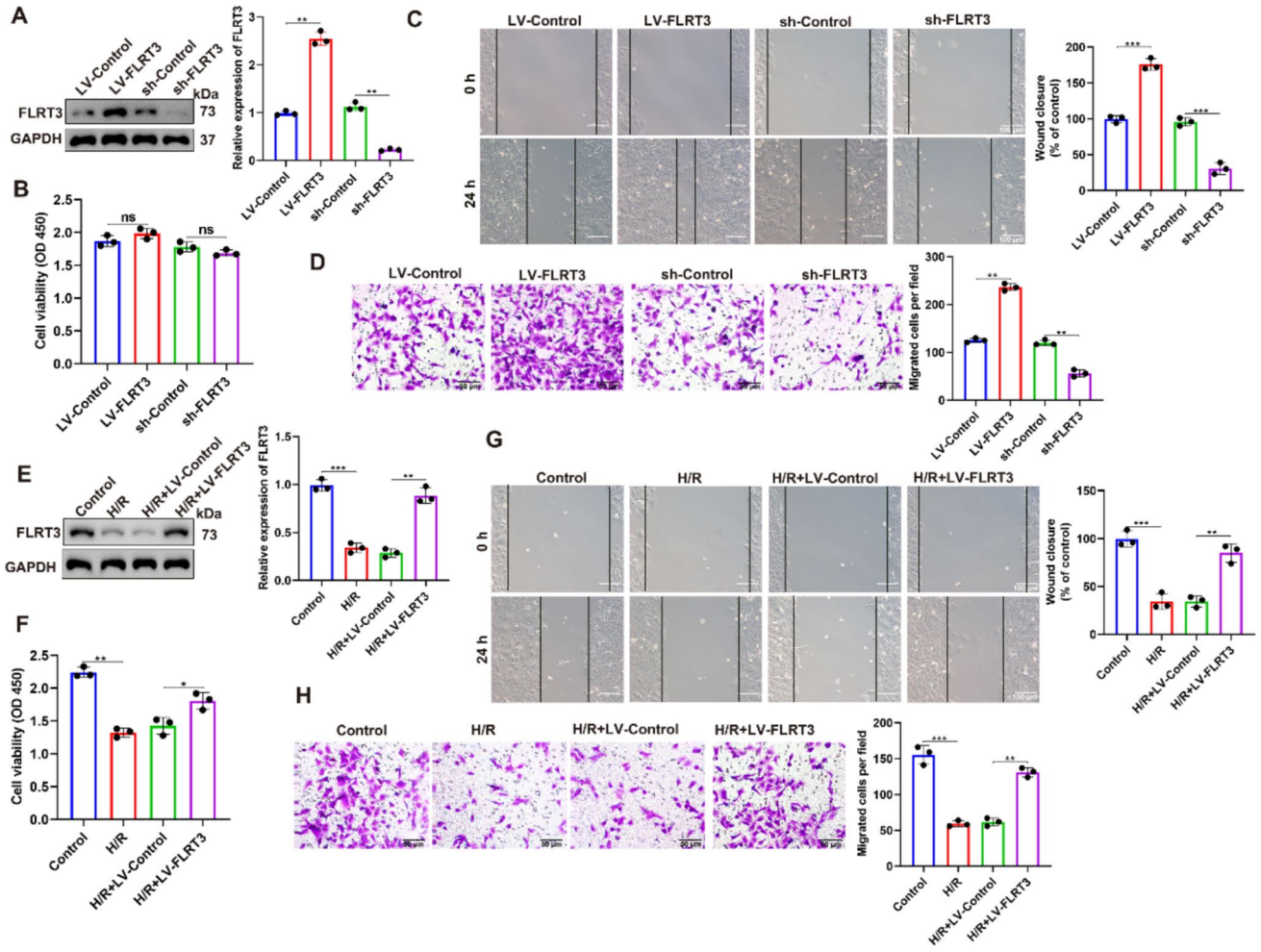

Fig. 2 Overexpression of FLRT3 promotes cell migration and rescues H/R-induced cell death and inhibition on cell migration. HPMECs were transduced with LV-Control, LV-FLRT3, sh-Control or sh-FLRT3 for 48 h. **A** Western blot confirmed successful FLRT3 overexpression and knockdown in HPMECs. **B** CCK-8 assay showed FLRT3 manipulation did not affect baseline cell viability. **C** Wound healing assay (24 h) demonstrated enhanced migration in LV-FLRT3 group and reduced migration in sh-FLRT3 group. **D** Transwell migration assay validated the migration changes with FLRT3 manipulation. **E** Western blot showed LV-FLRT3 restored H/R-induced FLRT3 reduction. **F** CCK-8 assay revealed FLRT3 overexpression protected against H/R-induced viability decrease. **G** Wound healing assay demonstrated FLRT3 overexpression preserved migration capacity under H/R conditions. **H** Transwell assay confirmed the protective effect of FLRT3 on H/R-impaired cell migration. Data are mean ± SD ($n = 3$/group). Statistical significance was determined using one-way ANOVA and Tukey's multiple comparisons test to compare multiple groups. $^{*}P < 0.05$, $^{**}P < 0.01$, $^{***}P < 0.001$ compared with the indicated groups

The integrity of the endothelial barrier is mediated through the cytoskeleton, which comprises actin microfilaments, microtubules and intermediate filaments. Thus, we next examined the effects of FLRT3 on endothelial barrier integrity by measuring changes in the endothelial cell cytoskeletal structure and cell–cell junctions. Immunofluorescence staining revealed that F-actin fibers, stained with FITC-phalloidin, were arranged regularly in control cells (Fig. 3C). However, H/R resulted in cytoskeletal remodeling characterized by a disorganized arrangement of F-actin stress fiber (Fig. 3C). Overexpression of FLRT3 was found to partially restore the cytoskeletal structure of H/R-treated cells (Fig. 3C).

The integrity of cell–cell junctions following H/R and FLRT3 overexpression was assessed by examining the protein expression levels of key components of adherens junctions including VE-cadherin, and tight junctions including claudin-5, occludin and ZO-1 [36]. Western blot analysis revealed that following H/R, VE-cadherin, claudin-5, ZO-1 and occludin protein expression levels were significantly decreased (Fig. 3D). However, overexpression of FLRT3 partially rescued this response. Immunofluorescence staining

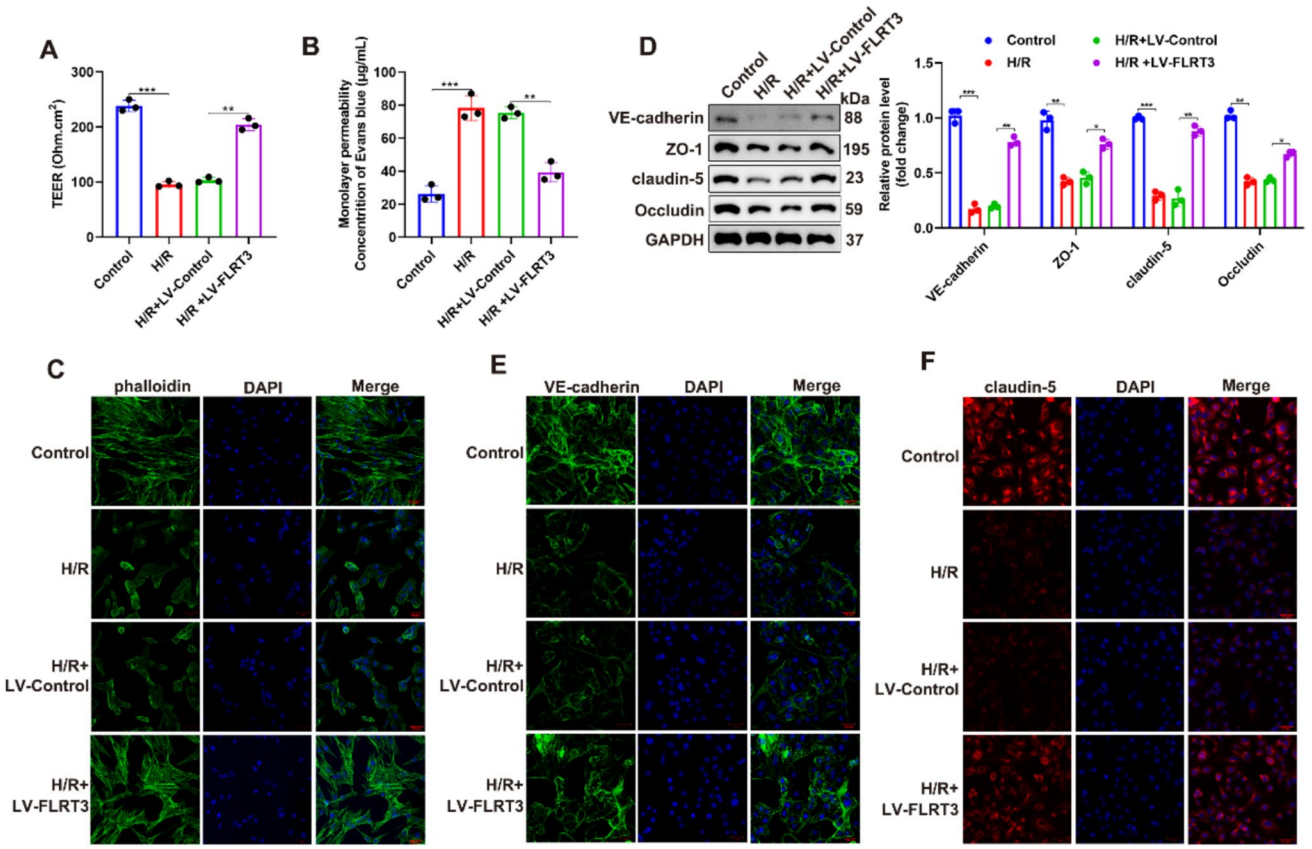

Fig. 3 FLRT3 overexpression increases endothelial barrier integrity via cytoskeletal remodeling and restoration of cell–cell junctions after H/R. HPMECs were transduced with LV-Control or LV-FLRT3 for 48 h, then subjected to H/R. **A** TEER measurements showed FLRT3 overexpression prevented H/R-induced barrier dysfunction. **B** Evans blue permeability assay demonstrated FLRT3 overexpression reduced H/R-induced barrier leakage. **C** F-actin staining (FITC-phalloidin, green; DAPI, blue) revealed FLRT3 overexpression maintained cytoskeletal organization under H/R. Scale bar, 50 μm. **D** Western blot showed FLRT3 overexpression preserved junction protein levels after H/R. **E** VE-cadherin immunofluorescence demonstrated maintained adherens junctions with FLRT3 overexpression during H/R. Scale bar, 50 μm. **F** Claudin-5 immunofluorescence showed preserved tight junction organization with FLRT3 overexpression after H/R. Data are mean ± SD ($n = 3$/group). Statistical significance was determined using one-way ANOVA and Tukey's multiple comparisons test. $^{*}P < 0.05$, $^{**}P < 0.01$, $^{***}P < 0.001$ compared with the indicated groups

of VE-cadherin (Fig. 3E) and claudin-5 (Fig. 3F) revealed similar results. Together, these findings suggest that FLRT3 has a role in mediating cell–cell junctions and cytoskeletal remodeling to improve endothelial barrier integrity.

FLRT3 Protein Is Destabilized After H/R

After confirming that FLRT3 protein expression levels were suppressed in H/R-treated HPMECs, we next sought to determine whether FLRT3 was downregulated via transcriptional regulation. qRT/PCR analysis revealed that FLRT3 mRNA levels remained unchanged in H/R cells (Fig. 4A) and I/R mice (Fig. 4B), suggesting that downregulation of FLRT3 in IRI was not regulated transcriptionally. To further determine whether downregulation of the FLRT3 protein occurred through translational or post-translational regulation, we next assessed the stability of FLRT3 by treating control and H/R cells with the protein synthesis inhibitor cycloheximide (CHX). We found that FLRT3 protein expression was stably maintained for 8 h in control cells but was dramatically reduced in H/R cells starting at 2 h after CHX treatment (Fig. 4C, D). These results suggest that FLRT3 is downregulated through destabilization of the FLRT3 protein in H/R cells.

In eukaryotic cells, protein degradation is mediated by two major pathways, the ubiquitin-proteasome pathway and lysosomal proteolysis. Thus, we next sought to determine whether FLRT3 protein was degraded through the ubiquitin–proteasome pathway in H/R cells by treating H/R cells with the proteasome inhibitor MG132. We found that inhibiting proteasome-mediated protein degradation did not prevent FLRT3 downregulation in H/R-treated HPMECs, suggesting that degradation of FLRT3 protein in H/R-treated HPMECs was proteasome-independent

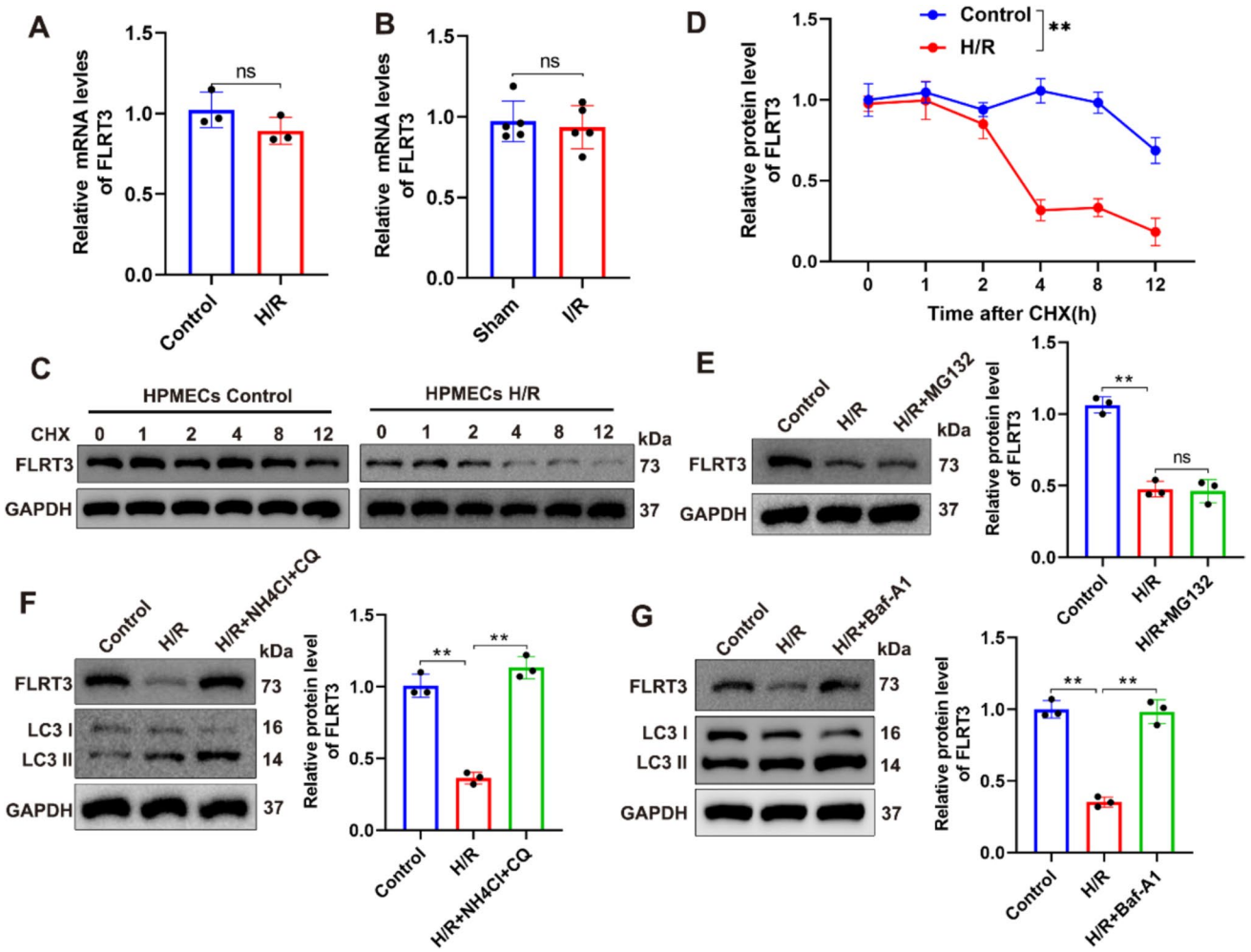

Fig. 4 The FLRT3 protein is destabilized through the autophagic–lysosomal pathway after H/R. **A** qRT-PCR revealed unchanged FLRT3 mRNA levels in HPMECs after H/R ($n=3$/group). **B** qRT-PCR showed stable FLRT3 mRNA levels in lung tissue after I/R ($n=5$/group). **C**, **D** Protein stability assay using CHX (20 μg/ml) demonstrated accelerated FLRT3 degradation in H/R-treated HPMECs, with significant reduction at 2 h post-CHX ($n=3$/group). **E** Western blot showed proteasome inhibitor MG132 (5 μM) failed to prevent H/R-induced FLRT3 degradation ($n=3$/group). **F** Lysosomal inhibitors NH_4Cl (10 μM) and CQ (10 μM) restored FLRT3 levels in H/R-treated HPMECs. Western blot quantification showed significant restoration of FLRT3 levels with both inhibitors ($n=3$/group). **G** Autophagy inhibitor Baf-A1 (100 nM) increased both LC3-II/LC3-I ratio and FLRT3 levels under H/R conditions ($n=3$/group). Data are presented as mean ± SD. Statistical significance was determined using unpaired Student's *t* test to compare two groups and one-way ANOVA and Tukey's multiple comparisons test to compare multiple groups. Two-way ANOVA with Tukey's post hoc test was used to compare multiple groups with two categorical variables. $^{**}P<0.01$ compared with the indicated groups. *Baf-A1* Bafilomycin-A1, *CHX* cycloheximide, *CQ* chloroquine, *NH_4Cl* ammonium chloride

(Fig. 4E). Next, we asked whether FLRT3 protein was degraded through the lysosomal pathway by treating H/R-treated HPMECs with the lysosome inhibitors ammonium chloride (NH_4Cl) and chloroquine (CQ) to inhibit the activity of lysosomal enzymes. We found that FLRT3 protein expression in H/R cells was restored by treatment with NH_4Cl and CQ (Fig. 4F), indicating that FLRT3 is downregulated through lysosome-mediated proteolysis. This observation prompted us to further investigate whether autophagy was involved in lysosome-mediated FLRT3 protein degradation. We next treated H/R-treated HPMECs with bafilomycin A1 (Baf-A1) to inhibit fusion between autophagosomes and lysosomes. Baf-A1 treatment of H/R-treated HPMECs resulted in the accumulation of autophagosomes as measured by an increase in LC3-II/LC3-I conversion, as well as an increase in FLRT3 protein expression levels (Fig. 4G). These data suggest that the degradation of FLRT3 in H/R-treated HPMECs occurs via the autophagic–lysosomal pathway.

RND3 Is a Target of FLRT3

We next sought to identify molecular mechanisms linking FLRT3 to the RhoA kinase pathway, which is a primary pathway associated with cytoskeletal rearrangement [37]. The HumanBase Gene Networks database predicted a correlation between FLRT3 and RND3 (also known as RhoE) in lung tissue (Fig. 5A), which was confirmed by co-IP (Fig. 5B) in HPMECs and GST pulldown (Fig. 5C) assays. Immunofluorescence staining indicated that FLRT3 colocalized with RND3 (Fig. 5D). Together, these results suggest that RND3 is a direct downstream target of FLRT3. Furthermore, western blot analysis demonstrated that overexpression of FLRT3 led to increased RND3 expression, while FLRT3 knockdown led to a reduction in RND3 expression (Fig. 5E). RND3 protein expression levels were significantly reduced following H/R, while overexpression of FLRT3 restored RND3 expression levels in H/R-treated cells (Fig. 5F). Together, our findings suggest that RND3 is a target of FLRT3 during H/R.

RND3 Is Required for FLRT3 Overexpression Related Migration and Endothelial Barrier Integrity in HPMEC Cells After H/R

To determine whether FLRT3 mediates its protective effects against H/R through RND3, we next examined the effects of FLRT3 overexpression and RND3 knockdown on the migration, endothelial cell barrier function, and cytoskeletal structure of H/R-induced HPMECs. As shown in Fig. 6A, H/R resulted in decreased FLRT3 and RND3 protein expression levels. Overexpression of FLRT3 led to an increase in RND3 protein expression, while knockdown of RND3 in FLRT3-overexpressing HPMECs resulted in a reduction in

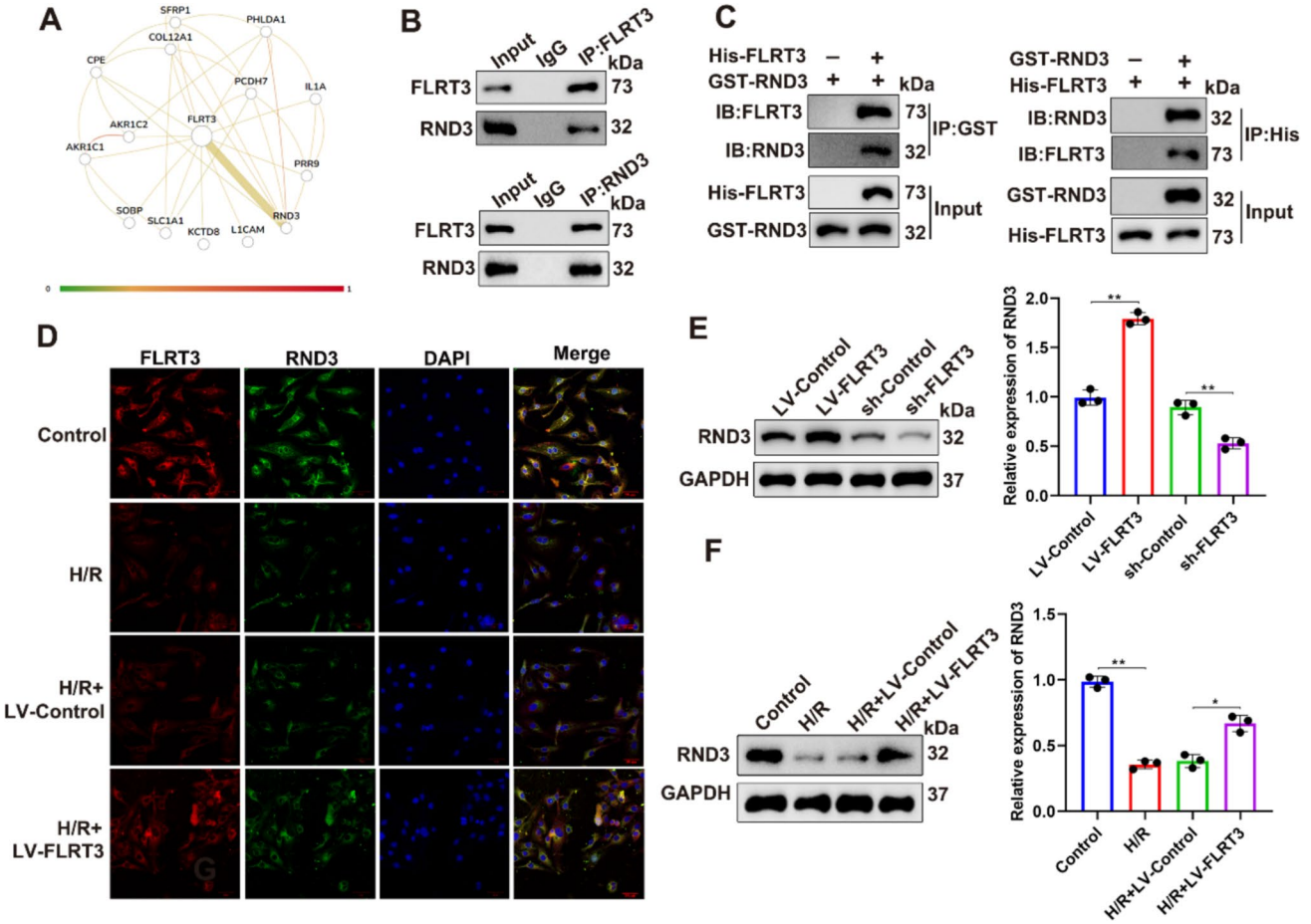

Fig. 5 RND3 is a target of FLRT3. **A** HumanBase Gene Networks analysis predicted functional correlation between FLRT3 and RND3 in lung tissue. **B** Co-IP assay demonstrated endogenous FLRT3–RND3 protein interaction in HPMECs, with input and IgG controls confirming specificity. **C** GST pulldown assay validated direct FLRT3-RND3 binding. **D** Double immunofluorescence (FLRT3-red, RND3-green) showed protein co-localization in HPMECs. Scale bar, 50 μm. **E** Western blot revealed FLRT3 overexpression increased RND3 levels while FLRT3 knockdown reduced RND3 expression. **F** Western blot showed FLRT3 overexpression restored H/R-induced RND3 reduction ($P < 0.01$). Data are mean ± SD ($n = 3$/group). Statistical significance was determined using one-way ANOVA and Tukey's multiple comparisons test. *$P < 0.05$, **$P < 0.01$ compared with the indicated groups

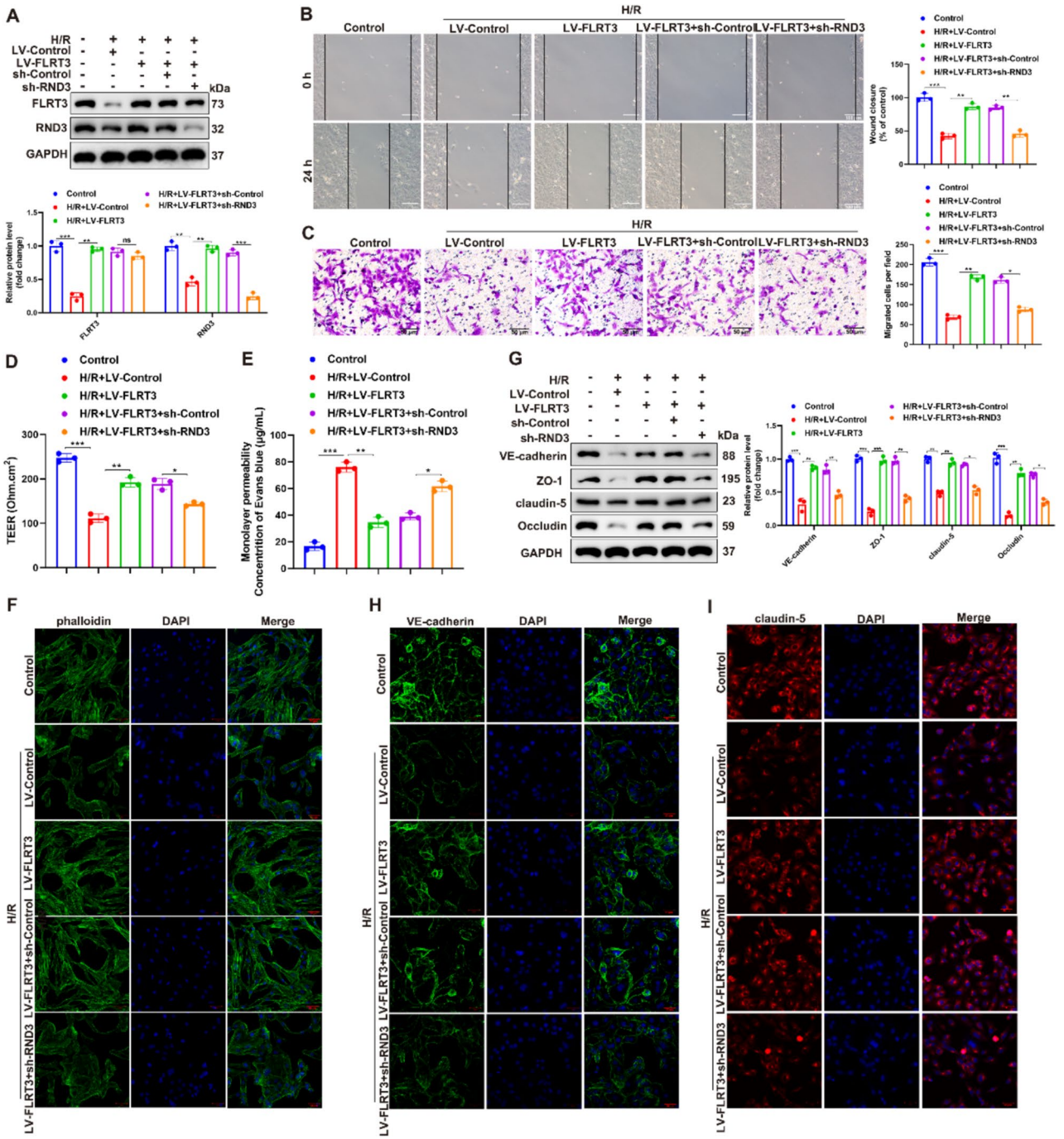

Fig. 6 RND3 is required for FLRT3 overexpression related cytoprotective effects after H/R in HPMEC cells. H/R-induced HPMECs were transduced with LV-FLRT3 and/or sh-RND3. **A** Western blot showed that overexpression of FLRT3 led to an increase in RND3 protein expression, while knockdown of RND3 in FLRT3-overexpressing HPMECs resulted in a reduction in RND3 protein expression levels. **B**, **C** Western blot showed RND3 knockdown reversed FLRT3-mediated protein expression under H/R. **D** TEER measurements revealed RND3 knockdown compromised FLRT3's barrier-protective effect. **E** Evans blue assay validated RND3's requirement in FLRT3-mediated barrier protection. **F** F-actin staining (phalloidin, green; DAPI, blue) showed RND3 knockdown prevented FLRT3's cytoskeletal preservation. Scale bar, 50 μm. **G** Western blot demonstrated RND3 knockdown reversed FLRT3's protection of junction proteins (VE-cadherin, ZO-1, claudin-5, and occludin). **H**, **I** Immunofluorescence of VE-cadherin (**H**) and claudin-5 (**I**) confirmed RND3's role in FLRT3-mediated junction maintenance. Scale bar, 50 μm. Data are mean ± SD ($n = 3$/group). Statistical significance was determined using one-way ANOVA and Tukey's multiple comparisons test. $^{*}P < 0.05$, $^{**}P < 0.01$, $^{***}P < 0.001$ compared with the indicated groups

RND3 protein expression levels. Wound healing and Transwell assays revealed that knockdown of RND3 reduced the protective effects of FLRT3 overexpression on cell migration in H/R-treated cells (Fig. 6B, C). Similarly, RND3 silencing reduced the protective effects of FLRT3 overexpression on endothelial barrier function (Fig. 6D) and vascular leakage (Fig. 6E) in H/R-treated cells. Immunofluorescence staining revealed that while overexpression of FLRT3 protected the cytoskeleton against H/R-induced injury, these protective effects were reduced when RND3 was downegulated (Fig. 6F). Western blot analysis of VE-cadherin, ZO-1, claudin-5 and occludin protein expression levels indicated that knockdown of RND3 reduced the protective effects of FLRT3 overexpression on cell–cell junctions in H/R-treated HPMECs (Fig. 6G). Similar results were observed by immunofluorescence staining of VE-cadherin and claudin-5 (Fig. 6H, I). Together, our findings show that FLRT3 mediates its protective effects against H/R-induced cellular injury through RND3.

Activation of RhoA Kinase Reduced FLRT3 Overexpression Related Cytoprotective Effects Induced by H/R in HPMEC Cells

The Rho GTPase family plays a crucial role in regulating cytoskeletal organization, cell migration, and cell cycle progression [37]. RhoA, as a key member of the Rho GTPase family, functions as a molecular switch cycling between an active GTP-bound state and an inactive GDP-bound state. When RhoA kinase is activated, it phosphorylates several downstream targets including myosin phosphatase target subunit 1 (MYPT1) and myosin light chain (MLC). MYPT1 is a regulatory subunit of myosin phosphatase that controls MLC phosphorylation, while MLC phosphorylation directly regulates actomyosin contractility and stress fiber formation. The coordinated actions of these molecules are critical for maintaining endothelial barrier integrity [32, 38]. Previous studies have demonstrated that RhoA regulates lipopolysaccharide-induced lung cell injury via the Wnt/β-catenin pathway [39], highlighting the importance of RhoA in lung injury. Interestingly, treatment with idiopathic pulmonary fibrosis drugs, such as nintedanib and pirfenidone, has been shown to decrease the fibrotic phenotype and RhoA activity by upregulating Rnd3 protein expression [40]. Given our findings that RND3 interacts with and acts downstream of FLRT3, we hypothesized that FLRT3 may protect HPMECs against H/R injury by suppressing the RhoA signaling pathway via RND3. Using pull-down assay and western blot analysis, we found that RhoA activity was significantly increased, accompanied by elevated phosphorylation of MYPT1 and MLC following H/R, while overexpression of FLRT3 significantly reduced this response (Fig. 7A). In addition, we found that RND3 knockdown reversed the effects of FLRT3 overexpression on RhoA activity, the phosphorylation of MYPT1 and MLC in H/R-treated cells (Fig. 7B), suggesting that FLRT3 may act via the RhoA kinase pathway. Next, we used the RhoA pathway agonist U-46619 to further determine whether FLRT3 mediates its protective effects via inhibition of the RhoA kinase pathway. We found that overexpression of FLRT3 protected against the H/R-induced inhibition of cell migration. However, treatment U-46619 blocked the effects of FLRT3 overexpression on cell migration (Fig. 7C, D). Similarly, U-46619 treatment blocked the protective effects of overexpressing FLRT3 on endothelial cell barrier function as measured by TEER (Fig. 7E) and vascular leakage as measured by the Evans blue dye assay (Fig. 7F). Finally, immunofluorescence staining with FITC-phalloidin, VE-cadherin and claudin-5 demonstrated that U-46619 treatment reduced the protective effects of FLRT3 overexpression on the cytoskeletal structure (Fig. 7G), adherens junctions (Fig. 7H) and tight junctions (Fig. 7I). Taken together, our data suggest that FLRT3 mediates its protective effects against H/R injury through inhibition of the RhoA kinase pathway.

Knockdown RND3 Reduces FLRT3 Overexpression Related Protective Effects on I/R-Induced Lung Injury in Mice

Finally, we sought to elucidate the mechanism of action of FLRT3 on I/R in vivo. RND3 protein levels were found to be significantly increased in the lung tissue of I/R mice treated with LV-FLRT3 compared to I/R mice (Fig. 8A). Consistent with our in vitro data, overexpression of FLRT3 led to an increase in VE-cadherin, claudin-5, ZO-1, and occludin protein expression levels in the lung tissue of I/R mice (Fig. 8B). Furthermore, FLRT3 overexpression reversed the effects of I/R on RhoA activity, the phosphorylation of MYPT1 and MLC (Fig. 8C). To investigate the role of RND3 in I/R, mice were treated with LV-FLRT3 and sh-RND3 via tail vein injection 3 days before I/R surgery by tail vein. Results showed that knockdown of RND3 on top of FLRT3 overexpression resulted in a significant decrease in RND3 protein expression (Fig. 8J). RND3 knockdown impaired the protective effect of FLRT3 overexpression as measured by changes in lung tissue injury (Fig. 8D), apoptosis (Fig. 8E), PaO_2/FiO_2 ratio (Fig. 8F) and lung wet-to-dry weight ratio (Fig. 8G). Evans blue dye assay indicated that RND3 silencing increased vascular permeability (Fig. 8H). TEM showed that RND3 silencing reduced the increased integrity of cell–cell junctions caused by LV-FLRT3 treatment of I/R mice (Fig. 8I). Finally, RND3 knockdown reversed the effects of FLRT3 overexpression on RhoA activity, the phosphorylation of MYPT1 and MLC in I/R mice (Fig. 8J). Together, our findings suggest that overexpression of FLRT3 can protect against I/R through RND3.

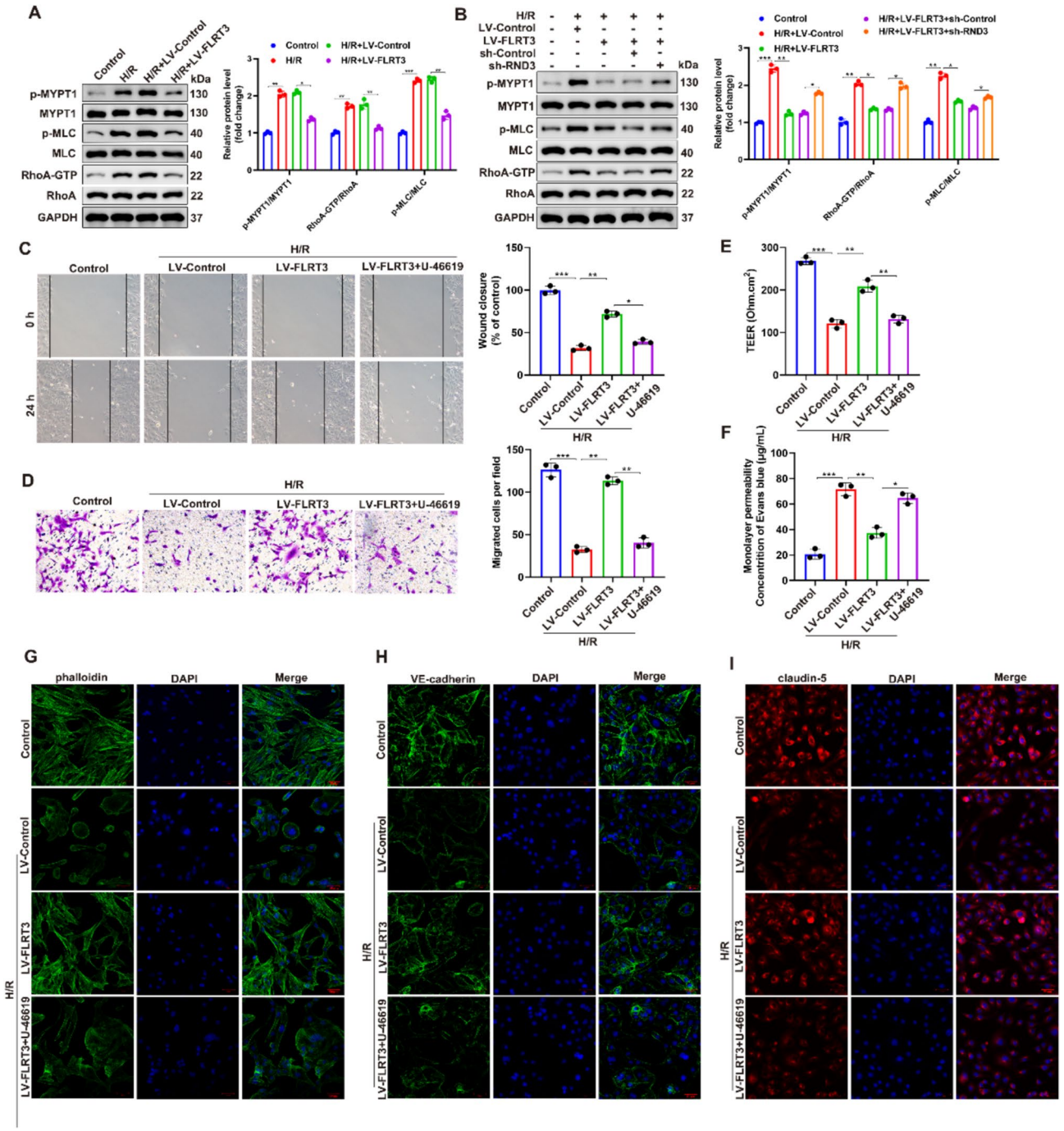

Fig. 7 Activation of RhoA kinase reduced FLRT3 overexpression related cytoprotective effects induced by H/R in HPMEC cells. **A** RhoA-GTP pulldown assay and Western blot showed FLRT3 overexpression reduced H/R-induced RhoA pathway activation (RhoA-GTP, p-MYPT1/MYPT1, p-MLC/MLC). **B** Pull-down assay and western blot analysis demonstrated RND3 knockdown reversed FLRT3's suppression of RhoA signaling under H/R. **C** Wound healing assay showed RhoA activator U-46619 blocked FLRT3's migration-protective effect. **D** Transwell assay confirmed U-46619's inhibition of FLRT3-mediated migration protection. **E** TEER measurements revealed U-46619 prevented FLRT3's barrier-protective effect. **F** Evans blue assay validated U-46619's disruption of FLRT3-mediated barrier protection. **G** F-actin staining (phalloidin, green; DAPI, blue) showed U-46619 prevented FLRT3's cytoskeletal preservation. Scale bar, 50 μm. **H**, **I** Immunofluorescence of VE-cadherin (**H**) and claudin-5 (**I**) demonstrated U-46619 abolished FLRT3's junction protection. Data are mean ± SD ($n = 3$/group). Statistical significance was determined using one-way ANOVA and Tukey's multiple comparisons test. $^{*}P < 0.05$, $^{**}P < 0.01$, $^{***}P < 0.001$ compared with the indicated groups

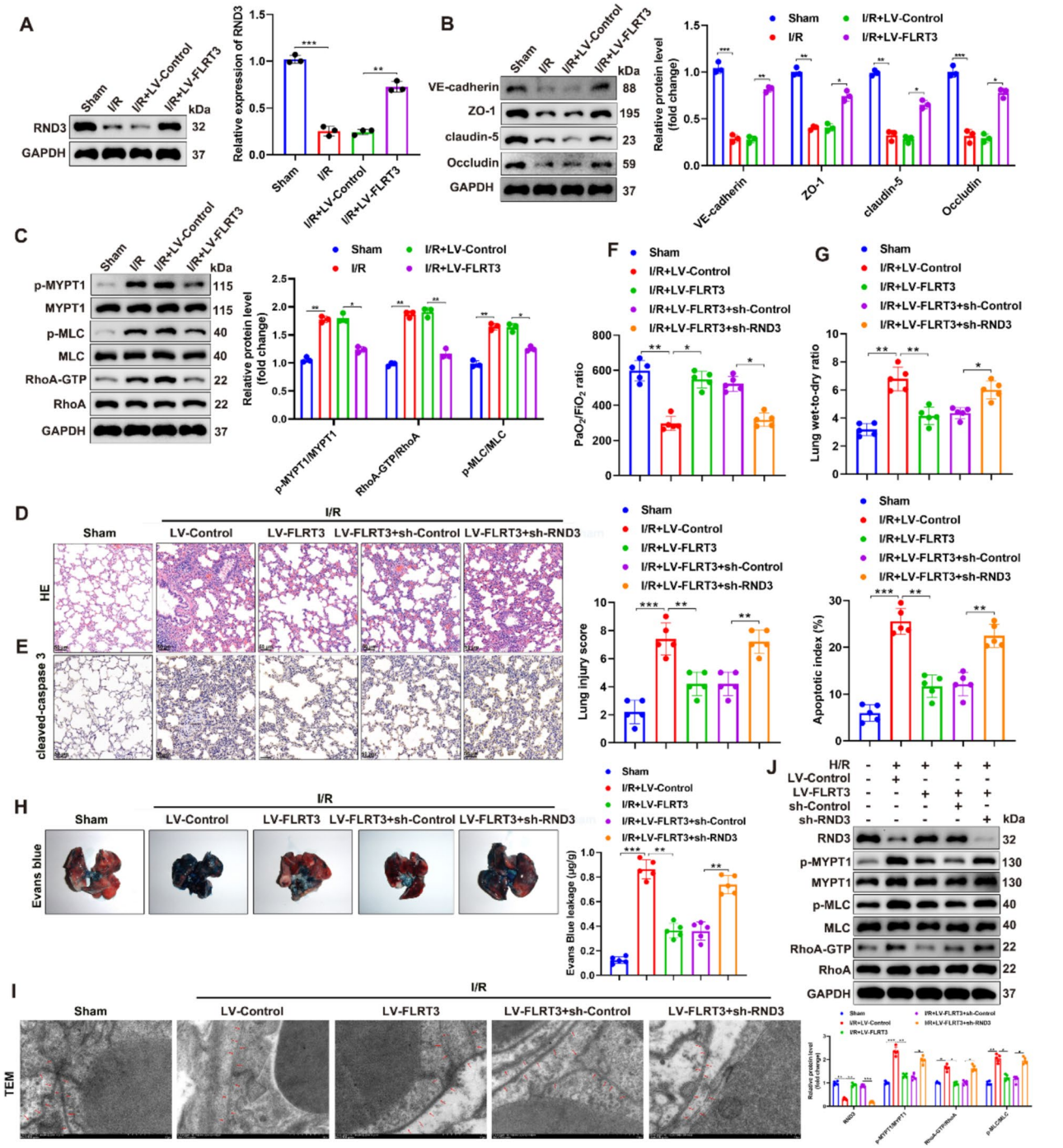

Fig. 8 Knockdown RND3 reduces FLRT3 overexpression related protective effects on I/R-induced lung injury in mice. **A-C** Analysis of lung tissue from mice receiving LV-FLRT3 via tail vein 3 days prior to I/R (60 min ischemia, 120 min reperfusion). **A** Western blot showing increased RND3 protein expression following FLRT3 overexpression. **B** Western blot demonstrating FLRT3-mediated restoration of junction proteins (VE-cadherin, claudin-5, ZO-1, and occludin). **C** Pull-down assay and western blot showing FLRT3-mediated suppression of RhoA pathway activation. **D–J** Analysis of lung tissue from mice treated with both LV-FLRT3 and sh-RND3 via tail vein 3 days before I/R surgery: **D** H&E staining showed RND3 knockdown reversed FLRT3's protection against tissue injury (quantified by injury scores). Scale bar, 50 μm. **E** Cleaved-caspase 3 immunohistochemistry demonstrated compromised anti-apoptotic effects. Scale bar, 50 μm. **F–H** I/R injury and vascular permeability revealed RND3 knockdown abolished FLRT3's protection via PaO_2/FiO_2 ratio (**F**), Lung wet/dry ratio (**G**), Evans blue extravasation (**H**). **I** TEM showed impaired endothelial junction preservation. **J** RhoA activity assays demonstrated restored RhoA pathway activation (RhoA-GTP, p-MYPT1, p-MLC). Data are mean ± SD ($n = 5$/group). $^{*}P < 0.05$, $^{**}P < 0.01$, $^{***}P < 0.001$ compared with the indicated groups

Discussion

Loss of endothelial barrier integrity and hyper-permeability of lung endothelial cells are known to play a central role in lung I/R injury [11–13]. FLRT3 is expressed on endothelial cells [33] and has previously been found to be the most downregulated gene in thoracic adipose tissue in human lung transplants [34]. This downregulation of FLRT3 in transplant settings suggests its potential importance in maintaining endothelial barrier function during I/R conditions, which prompted our investigation into its role in lung I/R injury.

Following I/R-induced endothelial barrier injury, repair of the endothelial barrier requires restoration of a functional endothelial monolayer and re-establishment of endothelial adherens and cell–cell tight junctions to reduce vascular leakage [27]. Our study demonstrates that FLRT3 plays a crucial role in these repair processes by promoting endothelial cell migration and restoring barrier integrity through the re-establishment of cytoskeletal structure and cell–cell junctions.

The most significant finding of our study is the identification of the molecular mechanism through which FLRT3 protects against I/R injury. The role of RhoA-GTPases in regulating the actin filament, endothelial barrier activity, cell adhesion and motility is well documented [24, 32, 38]. We demonstrate that FLRT3 functions through RND3, a regulator of actin cytoskeleton dynamics and cellular migration [41–43]. Our results reveal that FLRT3 overexpression inhibits H/R-induced activation of the RhoA kinase pathway, with this protective effect being blocked by RhoA agonist treatment. These mechanistic findings were further validated in our mouse model of I/R, where RND3 silencing impaired the protective effects of FLRT3 overexpression. The therapeutic implications of these findings are particularly promising, as previous studies have established the potential of Rho kinase inhibitors in treating acute lung injury [44] and restoring endothelial barrier function [32]. Moreover, RND3 has demonstrated therapeutic potential in reducing microvascular leakage and promoting endothelial barrier recovery in inflammatory conditions [45, 46]. Thus, our identification of FLRT3 as an upstream regulator of this pathway provides a novel therapeutic target for lung I/R injury.

Several limitations of our study should be acknowledged. While our immunofluorescence staining revealed FLRT3 expression was predominantly localized in large vessels of the lung, and I/R injury primarily affects small vessels and the microvasculature, our findings suggest that enhancing large vessel barrier function through FLRT3 may help maintain overall vascular homeostasis and compensate for microvascular injury. Nevertheless, this differential distribution pattern warrants further investigation to fully understand how FLRT3's vessel-specific expression pattern influences its protective effects across different vascular compartments during I/R injury. Additionally, while our findings demonstrate the protective effects of FLRT3 overexpression, the optimal timing and dosing of FLRT3 intervention need further investigation. Our study focused on acute I/R injury, and the long-term effects of FLRT3 manipulation remain to be determined. The potential side effects of FLRT3 overexpression in other organs also need to be evaluated before clinical application.

Future studies should address several key questions. First, the development of small molecule modulators of FLRT3 or its downstream pathways could provide more practical therapeutic options than viral vectors. Second, investigation of FLRT3's role in other types of lung injury might broaden its therapeutic applications. Moreover, detailed studies on FLRT3's expression and function in different-sized vessels could help optimize its therapeutic targeting and better understand its compensatory mechanisms in preserving pulmonary vascular integrity. Finally, clinical studies are needed to validate these findings in human patients and determine the feasibility of FLRT3-based therapies.

In conclusion, our study identifies FLRT3 as a novel therapeutic target for lung I/R injury through its regulation of the RND3/RhoA pathway. The protective effects of FLRT3 on endothelial barrier function suggest its potential as a preventive treatment for lung I/R injury, though further clinical studies are needed to validate these findings in patients.

Author Contributions Conceptualization, Y.Z.; Data curation, F.P.; Formal analysis, C.J.; Project administration, S.Y.S and Y.C.L; Supervision, J.W.S.; Visualization, Q.T.; Writing – original draft, Y.M.C.; Writing – review & editing, W.F.H. and Y.C.L.

Funding This work was financially supported by the National Natural Science Foundation of China (82272245); Natural Science Foundation of Shanghai (21Y11902800); Technical standardization management and promotion project of Shanghai Shenkang Hospital Development Center (SHDC22023211); Clinical technology innovation project of Shanghai Shenkang Hospital Development Center (SHDC22021203, SHDC12022121); Shanghai Chongming District Sustainable Development and Technological Innovation Action Plan Project (CKY2024-36); Exploration of the Application of Quality Management Tools in Intensive Care Medicine Education under the Context of High-Quality Development (2024-B-12).

Data Availability The data that support the findings of this study are available from the authors, upon reasonable request.

Declarations

Conflict of Interest The authors declare that they have no competing interests.

Ethics Approval The study was conducted according to the guidelines of the Declaration of Helsinki, and approved by the Ethics Commit-

tee of Shanghai Tenth People's Hospital, Tongji University School of Medicine (Approval Number: SHDSYY-2022-6500).

References

1. Pinto A et al (2016) The extracellular isoform of superoxide dismutase has a significant impact on cardiovascular ischaemia and reperfusion injury during cardiopulmonary bypass. Eur J Cardiothorac Surg 50:1035–1044. https://doi.org/10.1093/ejcts/ezw216
2. Randhawa SK, Roberts SH, Puri V (2022) Disparities in lung transplantation. Thorac Surg Clin 32:51–55. https://doi.org/10.1016/j.thorsurg.2021.09.001
3. Capuzzimati M, Hough O, Liu M (2022) Cell death and ischemia-reperfusion injury in lung transplantation. J Heart Lung Transplant 41:1003–1013. https://doi.org/10.1016/j.healun.2022.05.013
4. Leung CH et al (2015) Remote ischemic conditioning prevents lung and liver injury after hemorrhagic shock/resuscitation: potential role of a humoral plasma factor. Ann Surg 261:1215–1225. https://doi.org/10.1097/sla.0000000000000877
5. Deng C et al (2015) Inflammatory response and pneumocyte apoptosis during lung ischemia-reperfusion injury in an experimental pulmonary thromboembolism model. J Thromb Thrombolysis 40:42–53. https://doi.org/10.1007/s11239-015-1182-x
6. Lohser J, Slinger P (2015) Lung injury after one-lung ventilation: a review of the pathophysiologic mechanisms affecting the ventilated and the collapsed lung. Anesth Analg 121:302–318. https://doi.org/10.1213/ane.0000000000000808
7. Criner RN, Clausen E, Cantu E (2021) Primary graft dysfunction. Curr Opin Organ Transplant 26:321–327. https://doi.org/10.1097/mot.0000000000000876
8. Weyker PD, Webb CA, Kiamanesh D, Flynn BC (2013) Lung ischemia reperfusion injury: a bench-to-bedside review. Semin Cardiothorac Vasc Anesth 17:28–43. https://doi.org/10.1177/1089253212458329
9. Laubach VE, Sharma AK (2016) Mechanisms of lung ischemia-reperfusion injury. Curr Opin Organ Transplant 21:246–252. https://doi.org/10.1097/mot.0000000000000304
10. Yang Q, He GW, Underwood MJ, Yu CM (2016) Cellular and molecular mechanisms of endothelial ischemia/reperfusion injury: perspectives and implications for postischemic myocardial protection. Am J Transl Res 8:765–777
11. Claesson-Welsh L (2015) Vascular permeability–the essentials. Ups J Med Sci 120:135–143. https://doi.org/10.3109/03009734.2015.1064501
12. Claesson-Welsh L, Dejana E, McDonald DM (2021) Permeability of the endothelial barrier: identifying and reconciling controversies. Trends Mol Med 27:314–331. https://doi.org/10.1016/j.molmed.2020.11.006
13. Probst CK, Montesi SB, Medoff BD, Shea BS, Knipe RS (2020) Vascular permeability in the fibrotic lung. Eur Respir J 56:1900100. https://doi.org/10.1183/13993003.00100-2019
14. Assaad S, Kratzert WB, Shelley B, Friedman MB, Perrino A Jr (2018) Assessment of pulmonary edema: principles and practice. J Cardiothorac Vasc Anesth 32:901–914. https://doi.org/10.1053/j.jvca.2017.08.028
15. Casey JD, Semler MW, Rice TW (2019) Fluid management in acute respiratory distress syndrome. Semin Respir Crit Care Med 40:57–65. https://doi.org/10.1055/s-0039-1685206
16. Jungraithmayr W (2020) Novel strategies for endothelial preservation in lung transplant ischemia-reperfusion injury. Front Physiol 11:581420. https://doi.org/10.3389/fphys.2020.581420
17. Karki P, Birukova AA (2021) Microtubules as major regulators of endothelial function: implication for lung injury. Front Physiol 12:758313. https://doi.org/10.3389/fphys.2021.758313
18. Belvitch P, Htwe YM, Brown ME, Dudek S (2018) Cortical actin dynamics in endothelial permeability. Curr Top Membr 82:141–195. https://doi.org/10.1016/bs.ctm.2018.09.003
19. Rho SS, Ando K, Fukuhara S (2017) Dynamic regulation of vascular permeability by vascular endothelial cadherin-mediated endothelial cell-cell junctions. J Nippon Med Sch 84:148–159. https://doi.org/10.1272/jnms.84.148
20. Kása A, Csortos C, Verin AD (2015) Cytoskeletal mechanisms regulating vascular endothelial barrier function in response to acute lung injury. Tissue Barriers 3:e974448. https://doi.org/10.4161/21688370.2014.974448
21. García-Ponce A, Citalán-Madrid AF, Velázquez-Avila M, Vargas-Robles H, Schnoor M (2015) The role of actin-binding proteins in the control of endothelial barrier integrity. Thromb Haemost 113:20–36. https://doi.org/10.1160/th14-04-0298
22. White WL (2011) Erratum to: why I hate the index finger. Hand (N Y) 6:233. https://doi.org/10.1007/s11552-011-9321-0
23. Reglero-Real N, Colom B, Bodkin JV, Nourshargh S (2016) Endothelial cell junctional adhesion molecules: role and regulation of expression in inflammation. Arterioscler Thromb Vasc Biol 36:2048–2057. https://doi.org/10.1161/atvbaha.116.307610
24. Kempers L, Driessen AJM, van Rijssel J, Nolte MA, van Buul JD (2021) The RhoGEF trio: a protein with a wide range of functions in the vascular endothelium. Int J Mol Sci 22:10168. https://doi.org/10.3390/ijms221810168
25. Cerutti C, Ridley AJ (2017) Endothelial cell-cell adhesion and signaling. Exp Cell Res 358:31–38. https://doi.org/10.1016/j.yexcr.2017.06.003
26. Radeva MY, Waschke J (2018) Mind the gap: mechanisms regulating the endothelial barrier. Acta Physiol (Oxf) 222:e12860. https://doi.org/10.1111/apha.12860
27. Evans CE, Iruela-Arispe ML, Zhao YY (2021) Mechanisms of endothelial regeneration and vascular repair and their application to regenerative medicine. Am J Pathol 191:52–65. https://doi.org/10.1016/j.ajpath.2020.10.001
28. Komarova YA, Kruse K, Mehta D, Malik AB (2017) Protein interactions at endothelial junctions and signaling mechanisms regulating endothelial permeability. Circ Res 120:179–206. https://doi.org/10.1161/circresaha.116.306534
29. Ridley AJ (2015) Rho GTPase signalling in cell migration. Curr Opin Cell Biol 36:103–112. https://doi.org/10.1016/j.ceb.2015.08.005
30. Hasan SS, Siekmann AF (2015) The same but different: signaling pathways in control of endothelial cell migration. Curr Opin Cell Biol 36:86–92. https://doi.org/10.1016/j.ceb.2015.07.009
31. Combedazou A et al (2020) Small GTPases orchestrate cell-cell communication during collective cell movement. Small GTPases 11:103–112. https://doi.org/10.1080/21541248.2017.1366965

32. Tesfamariam B (2023) Targeting Rho kinase to restore endothelial barrier function following vascular scaffold implantation. Drug Discov Today 28:103609. https://doi.org/10.1016/j.drudis.2023.103609
33. Jauhiainen S et al (2019) Axon guidance-related factor FLRT3 regulates VEGF-signaling and endothelial cell function. Front Physiol 10:224. https://doi.org/10.3389/fphys.2019.00224
34. Diamond JM et al (2017) Adipose gene expression profile changes with lung allograft reperfusion. Am J Transplant 17:239–245. https://doi.org/10.1111/ajt.13964
35. Fei L, Jifeng F, Tiantian W, Yi H, Linghui P (2017) Glycyrrhizin ameliorate ischemia reperfusion lung injury through downregulate TLR2 signaling cascade in alveolar macrophages. Front Pharmacol 8:389. https://doi.org/10.3389/fphar.2017.00389
36. Hellenthal KEM, Brabenec L, Wagner NM (2022) Regulation and dysregulation of endothelial permeability during systemic inflammation. Cells 11:1935. https://doi.org/10.3390/cells11121935
37. Crosas-Molist E et al (2022) Rho GTPase signaling in cancer progression and dissemination. Physiol Rev 102:455–510. https://doi.org/10.1152/physrev.00045.2020
38. Beckers CM, van Hinsbergh VW, van Nieuw Amerongen GP (2010) Driving Rho GTPase activity in endothelial cells regulates barrier integrity. Thromb Haemost 103:40–55. https://doi.org/10.1160/th09-06-0403
39. Chen G, Sun X, Dong C (2017) RhoA regulates lipopolysaccharide-induced lung cell injury via the Wnt/β-catenin pathway. Mol Med Rep 16:8501–8506. https://doi.org/10.3892/mmr.2017.7662
40. Monaghan-Benson E, Wittchen ES, Doerschuk CM, Burridge K (2018) A Rnd3/p190RhoGAP pathway regulates RhoA activity in idiopathic pulmonary fibrosis fibroblasts. Mol Biol Cell 29:2165–2175. https://doi.org/10.1091/mbc.E17-11-0642
41. Jie W et al (2015) Pathophysiological functions of Rnd3/RhoE. Compr Physiol 6:169–186. https://doi.org/10.1002/cphy.c150018
42. Klein RM, Aplin AE (2009) Rnd3 regulation of the actin cytoskeleton promotes melanoma migration and invasive outgrowth in three dimensions. Cancer Res 69:2224–2233. https://doi.org/10.1158/0008-5472.Can-08-3201
43. Riou P, Villalonga P, Ridley AJ (2010) Rnd proteins: multifunctional regulators of the cytoskeleton and cell cycle progression. BioEssays 32:986–992. https://doi.org/10.1002/bies.201000060
44. Abedi F, Hayes AW, Reiter R, Karimi G (2020) Acute lung injury: the therapeutic role of Rho kinase inhibitors. Pharmacol Res 155:104736. https://doi.org/10.1016/j.phrs.2020.104736
45. Breslin JW et al (2016) Rnd3 as a novel target to ameliorate microvascular leakage. J Am Heart Assoc 5:e003336. https://doi.org/10.1161/jaha.116.003336
46. Basbous S, Azzarelli R, Pacary E, Moreau V (2021) Pathophysiological functions of Rnd proteins. Small GTPases 12:336–357. https://doi.org/10.1080/21541248.2020.1829914